Comprehensive investigation of the symmetric space-star configuration in the nucleon-deuteron breakup

H. Witała,[1,*] J. Golak,[1] R. Skibiński,[1] K. Topolnicki,[1] E. Epelbaum,[2] H. Krebs,[2] and P. Reinert[2]
[1]*M. Smoluchowski Institute of Physics, Jagiellonian University, PL-30348 Kraków, Poland*
[2]*Institut für Theoretische Physik II, Ruhr-Universität Bochum, D-44780 Bochum, Germany*

(Received 19 February 2021; accepted 24 June 2021; published 6 July 2021)

We examine a description of available cross section data for symmetric space star (SST) configurations in the neutron-deuteron (*nd*) and proton-deuteron (*pd*) breakup reaction using numerically exact solutions of the three-nucleon (3*N*) Faddeev equation based on two- and three-nucleon (semi)phenomenological and chiral forces. The predicted SST cross sections are very stable with respect to the underlying dynamics for incoming nucleon laboratory energies below ≈25 MeV. We discuss possible origins of the surprising discrepancies between theory and data found in low-energy *nd* and *pd* SST breakup measurements.

DOI: 10.1103/PhysRevC.104.014002

I. INTRODUCTION

Since the advent of numerically exact 3*N* continuum Faddeev calculations, the elastic nucleon-deuteron (*Nd*) scattering and deuteron breakup reactions have become a powerful tool to test modern models of nuclear forces [1–3]. With the appearance of high-precision (semi)phenomenological nucleon-nucleon (*NN*) potentials and first models of the 3*N* force (3NF) the question about the importance of the 3NF has become the main topic of studies in the 3*N* system. That issue was given a new impetus from chiral perturbation theory (ChPT), which opened the possibility to employ consistent two- and many-body nuclear forces derived within this framework in 3*N* continuum calculations.

First applications of (semi)phenomenological *NN* and 3*N* forces to elastic *Nd* scattering and to the nucleon-induced deuteron breakup reactions revealed interesting cases of discrepancies between theoretical predictions based solely on two-nucleon (2*N*) potentials and data, indicating a possibility of large 3NF effects [4,5]. The exclusive breakup reaction offers a rich spectrum of kinematically complete geometries and the symmetric space star (SST) configuration from the very beginning attracted attention as a possible candidate to reveal significant 3NF effects. In this kinematically complete geometry of *Nd* breakup the momenta of the three outgoing nucleons have the same magnitudes and they form a three-pointed "Mercedes-Benz" star perpendicular to the beam direction in the 3*N* center-of-mass (c.m.) frame. Measurements of the *pd* and *nd* breakup performed at low incoming nucleon energies in different laboratories indeed revealed large discrepancies between predicted theoretical cross sections and data for that geometry. The SST measurements for *nd* breakup have been performed at the following energies: $E = 10.25$ MeV Bochum [6], $E = 10.5$ MeV Erlangen [7] and TUNL [8], $E = 13.0$ MeV Erlangen [9,10] and TUNL [8,11,12], $E = 16.0$ MeV TUNL [13,14], $E = 19.0$ MeV TUNL [14], and $E = 25.0$ MeV CIAE [15]. For the corresponding *pd* breakup reaction, data were taken at $E = 10.5$ MeV Köln [16], $E = 13.0$ MeV Köln [17] and Fukuoka [18,19], $E = 19.0$ MeV Köln [20], and $E = 65.0$ MeV PSI [21]. The data provided by different groups at the same energy are consistent with each other both for the *pd* and *nd* systems, with *nd* SST cross sections clearly different from and larger than the *pd* ones.

The first analyses of the data performed in the framework of the 3*N* Faddeev formalism with the Bonn and Paris potentials [22,23] showed that theory underpredicted the low-energy SST *nd* cross sections while simultaneously overpredicting the *pd* ones. The development of *NN* potentials resulted in the construction of high-precision (semi)phenomenological interactions, such as Av18 [24], CD-Bonn [25], Nijm1, and Nijm2 [26], and their application in 3*N* continuum calculations confirmed the SST discrepancies between theory and data found with the older potentials. Further progress in numerical techniques permitted to include the 3NF in 3*N* Faddeev calculations [27] and first reported results with standard 3NF models such as Urbana IX [28] or 2π-exchange Tucson-Melbourne (TM99) [29] exhibited only moderate 3NF effects [4,5] at low energies.

All analyses of the *pd* breakup performed by the Cracow-Bochum group have a permanent drawback: they neglected the proton-proton (*pp*) long-range Coulomb interaction present in the *pd* system and were based on *nd* calculations. The successful implementation of the long-range proton-proton (*pp*) Coulomb force in the Faddeev formalism achieved in Ref. [30] permitted, for the first time, to perform exact calculations of *pd* breakup. It turned out that the *pp* Coulomb interaction effects are practically negligible for the SST cross sections [30], which validated the results of analyses of that geometry in *pd* breakup based on *nd* calculations.

Recent progress in constructing nuclear forces within chiral effective-field theory [31–33] resulted in several high-precision *NN* potentials. Also, for the first time, a possibility appeared of applying 2*N* and 3*N* forces derived consistently

*henryk.witala@uj.edu.pl

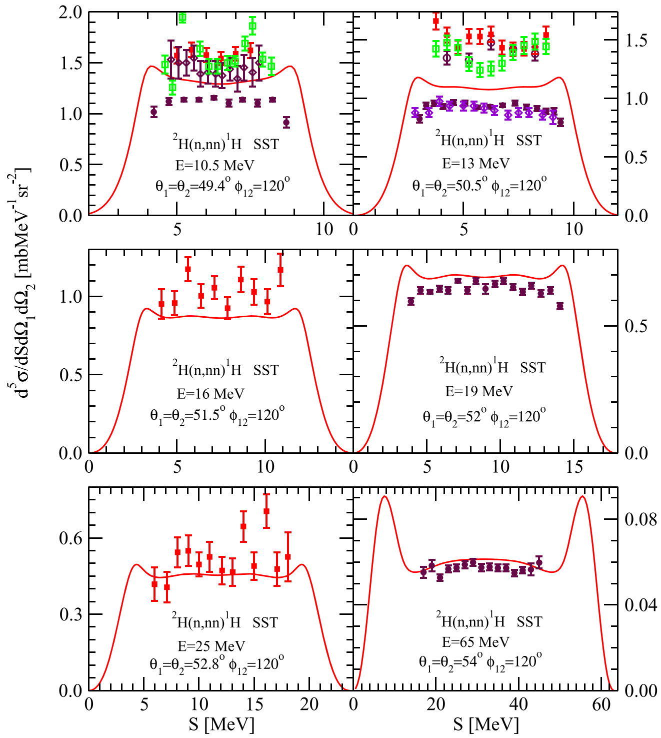

FIG. 1. The *nd* breakup fivefold differential cross section in the SST complete geometry at the incoming neutron laboratory energies $E = 10.5$, 13, 16, 19, 25, and 65 MeV, shown as a function of arclength of the S curve. The solid red lines are predictions of the CD Bonn *NN* potential. At $E = 10.5$ MeV the red squares, the maroon diamonds, and the green squares are 10.3 MeV TUNL [8], 10.25 MeV Bochum [6], and 10.5 MeV Erlangen [7] *nd* data, respectively. The maroon circles are 10.5 MeV Köln [16] *pd* data. At $E = 13$ MeV the red squares, the maroon circles, and the green squares are 13 MeV TUNL [12], 13 MeV TUNL [8], and 13 MeV Erlangen [9] *nd* data. The maroon circles are 13 MeV Köln [17] and violet diamonds 13 MeV Fukuoka [18] *pd* data. At $E = 16$ and 25 MeV the red squares are TUNL [13] and CIAE [15] *nd* data. The maroon circles at $E = 19$ and 65 MeV are Köln [20] and PSI [21] *pd* data.

within the same formalism. Understanding of nuclear spectra and reactions based on these consistent chiral two- and many-body forces has grown into a main topic of present day few-nucleon and many-nucleon studies.

In view of these new developments it is timely to check if it is possible to get new insights about the origin of the discrepancies between theory and data for the SST configuration by using the newly developed chiral two- and three-body interactions.

This paper is organized as follows: in Sec. II we present the available SST data together with their description by (semi)phenomenological forces and additionally discuss sensitivity of the SST cross sections to particular *NN* force components. Results with chiral *NN* potentials alone are presented in Sec. III, while in Sec. IV the importance of 3NF is discussed. In Sec. V we surmise on possible origins for the low-energy discrepancies between theoretical predictions and SST cross-section data. We summarize and conclude in Sec. VI.

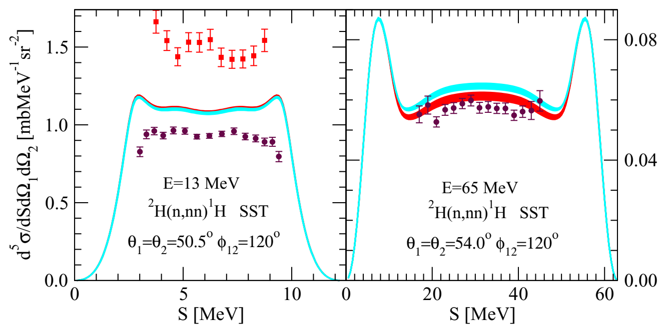

FIG. 2. The same as in Fig. 1 for the incoming neutron laboratory energies $E = 13$ and 65 MeV. The red dark shaded and cyan light shaded bands comprise predictions of the AV18, CD Bonn, Nijm1, and Nijm2 *NN* potentials alone or combined with TM99 and for AV18 also with Urbana IX 3NF, respectively. At $E = 13$ MeV the red squares are TUNL [12] *nd* data and the maroon circles are Köln [20] *pd* data. The maroon circles at $E = 65$ MeV are PSI [21] *pd* data.

II. RESULTS WITH (SEMI)PHENOMENOLOGICAL FORCES

Theoretical predictions which are shown in the present paper are obtained within the 3*N* Faddeev formalism using various 2*N* and 3*N* forces. The formalism itself and information regarding our numerical performance were presented in numerous publications, so for details we refer the reader to Refs. [1,27,34,35].

In Fig. 1 we show the available *Nd* SST cross-section data and compare them to theory based on the CD Bonn *NN* potential [25]. It is seen that, at low laboratory energies *E* of the incoming nucleon, theoretical predictions clearly underestimate *nd* data by ≈15%–30% and simultaneously overestimate *pd* data by ≈10%. The difference between theory and data decreases with growing energy, and, at $E = 65$ MeV, theory describes the *pd* data.

The predicted low-energy SST cross sections do not change when instead of the CD Bonn potential another (semi)phenomenological interaction is used. The very narrow red dark shaded band at 13 MeV in Fig. 2, which comprises AV18 [24], CD Bonn [25], and Nijm1 and Nijm2 [26] predictions, reflects the astonishing stability of the low-energy SST cross section to the underlying dynamics. This stability is lost at 65 MeV as evinced by broadening of the band showing the predictions with *NN* interactions only.

The predicted low-energy SST cross sections are not only stable with respect to the underlying *NN* (semi)phenomenological potentials but are also insensitive to the standard 2π-exchange 3NF's. In Fig. 2 we show also (cyan) light shaded bands containing predictions based on the AV18, CD Bonn, Nijm1, and Nijm2 interactions combined with the 2π-exchange Tucson-Melbourne (TM99) 3NF [29]. The cutoff parameter Λ of that 3NF is adjusted for each particular *NN* potential and the TM99 3NF combination to reproduce the experimental triton binding energy [4]. In Fig. 2 the band of $NN + 3$NF predictions contains also the cross section for the combination of the AV18 potential and the Urbana IX 3NF [28]. At 13 MeV, effects of these 3NF's

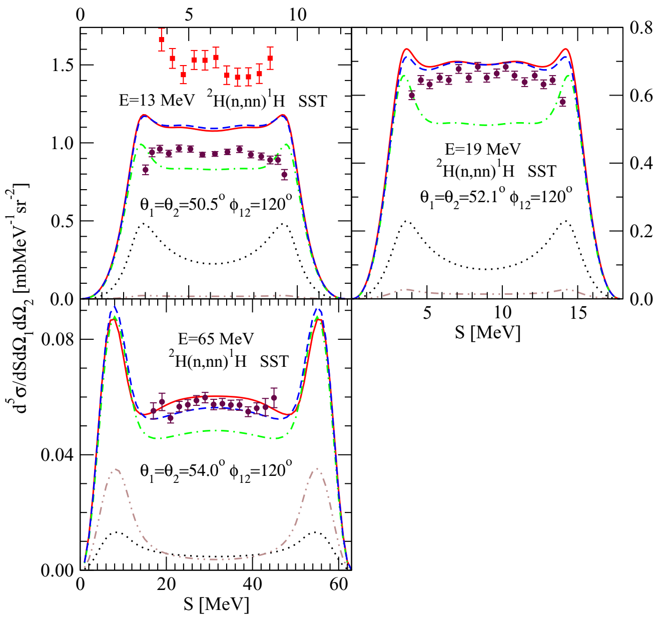

FIG. 3. Contributions to the SST cross section at $E = 13$, 19, and 65 MeV from different partial waves. The red solid line is prediction of the CD Bonn NN potential. The black dotted, and green dash-dotted lines show cross sections obtained with $3N$ partial waves restricted to these which contain only $^1S_0$ and $^3S_1 - {}^3D_1$ NN partial waves, respectively. The result obtained with only $^1S_0 + {}^3S_1 - {}^3D_1$ is given by blue dashed lines and prediction with all partial waves excluding $^1S_0 + {}^3S_1 - {}^3D_1$ is shown by brown dash-double-dotted lines. The maroon circles at $E = 19$ MeV are pd Köln data [20]. For a description of the data points at 13 and 65 MeV, see Fig. 2.

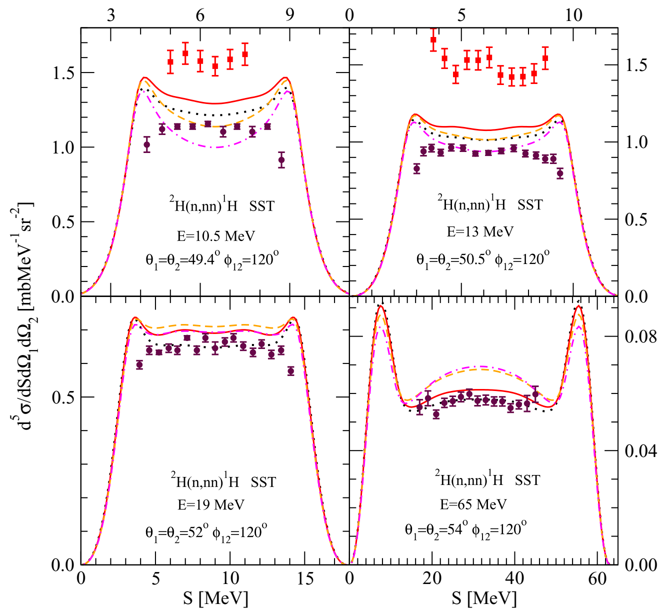

FIG. 4. Sensitivity of the SST cross section at $E = 10.5$, 13, 19, and 65 MeV to changes of the $^1S_0$ nn force component. The red solid line is prediction of the CD Bonn potential. The (black) dotted curve is the corresponding cross section when the strength of the nn $^1S_0$ force component is reduced by multiplying its matrix elements with a factor $\lambda = 0.9$. The orange dashed and magenta dash-dotted lines shows the cross section when that strength is increased by multiplying with factor $\lambda = 1.21$ and $\lambda = 1.3$, respectively. For a description of the data points, see Fig. 1.

are practically negligible, and the resulting band of predictions is very narrow and overlaps with the band representing NN-only predictions. The astonishing stability with respect to the underlying dynamics present at low energies is lost at 65 MeV. Here, both bands broaden significantly and slightly move apart, indicating small effects of the 3NF. It is a region of energy where, also in elastic Nd scattering, 3NF effects start coming into play [4,36].

The small effects of the 3NF and insensitivity to the underlying dynamics raise the question about the dominant NN force components, contributing to the SST cross section. It turns out that, at low energies, practically the whole input stems from the $^1S_0$ and $^3S_1$ NN force components only, with a dominating $^3S_1$ contribution (see Fig. 3). These force components provide nearly the whole cross section at low energies, as evinced by nearly overlapping red solid (CD Bonn prediction) and blue dashed (CD Bonn restricted to $^1S_0 + {}^3S_1 - {}^3D_1$ NN partial waves only) lines at 13 and 19 MeV in Fig. 3. With increasing energy the contributions from the remaining partial waves become visible and at 65 MeV they start to outweigh the $^1S_0$ part.

The low-energy dominance of the $^3S_1$ and $^1S_0$ contributions brings up the question to what extent uncertainties of these NN force components could be responsible for the observed discrepancies between theory and data. To answer this question we investigated changes of the SST cross section caused by varying the strengths of the $^3S_1$ and $^1S_0$ NN force components. To this end we multiplied the corresponding potential matrix elements by a factor λ. It was shown in Ref. [37] that changes of the $^1S_0$ interaction induced by the λ values in a vicinity of $\lambda = 1$ do not significantly affect exclusive Nd elastic-scattering observables and the total cross sections.

In the first step, we investigated what changes of the $^1S_0$ nn or pp interaction are required to get a proper description of the low-energy SST cross-section data. It turned out that it was not possible to modify the $^1S_0$ nn or pp potential in a way which would shift the cross-section predictions to the nd SST data. However, increasing the strength of $^1S_0\,nn$ interaction by ≈20%–30% brings theoretical predictions close to the pd SST cross sections at low energies (see Fig. 4). Such a large increase of the strength ($\lambda = 1.21$ or $\lambda = 1.3$) allows two neutrons to form a $^1S_0$ bound state with the binding energy $E_b^{\lambda=1.21} = -0.144$ MeV or $E_b^{\lambda=1.3} = -0.441$ MeV. Existence of such a dineutron state does not spoil the description of nd elastic-scattering data [37] but it would have severe consequences for the ^{3}H binding energy, increasing it from the CD Bonn value $E_{^3H}^{\text{CD Bonn}} = -7.923$ MeV to $E_{^3H}^{\lambda=1.21} = -9.717$ MeV or $E_{^3H}^{\lambda=1.3} = -10.560$ MeV. Admittedly, one could argue that an action of repulsive 3NFs could provide again proper binding of that system. However, such a strong $^1S_0$ force would also spoil the description of nuclear structure. As can be seen in Fig. 4, such modifications of the $^1S_0$ nn force

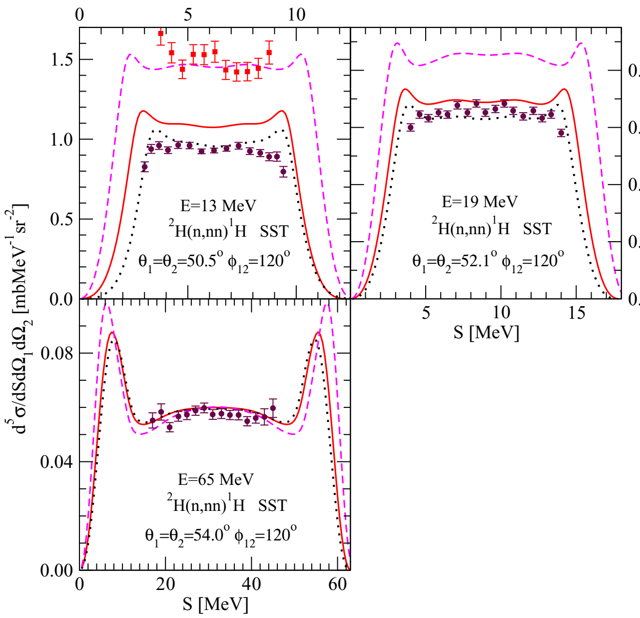

FIG. 5. Sensitivity of the SST cross section at $E = 13$, 19, and 65 MeV to changes of the $^3S_1 - {}^3D_1$ np force component. The red solid line is prediction of the CD Bonn potential. The magenta dashed curve is the corresponding cross section when the strength of that force component is reduced by 5% by multiplying its matrix elements with a factor $\lambda = 0.95$. The black dotted line shows the cross section when that strength is increased by 2% by multiplying matrix elements with the factor $\lambda = 1.02$. For a description of the data points, see Fig. 4.

component would also lead to a significant overestimation of the pd SST cross-section data at $E = 65$ MeV but this could change upon including the 3NF tuned to the ^{3}H binding energy.

In the case of the $^3S_1$ component, a proper description of nd SST data would require a reduction of its strength by $\approx 5\%$ ($\lambda = 0.95$; see Fig. 5), which leads to a complete deterioration of the np data description and to a deuteron binding energy $E_d^{\lambda=0.95} = -1.412$ MeV, drastically different from the experimental value $E_d^{\rm expt} = -2.224\,575(9)$ MeV [38]. Furthermore, ^{3}H would be bound by only $E_{^3H}^{\lambda=0.95} = -6.338$ MeV and a large effect of an attractive 3NF would be required to regain the CD Bonn ^{3}H binding. On the other hand, the SST pd data require only a 2% increase of $^3S_1 - {}^3D_1$ strength ($\lambda = 1.02$) (see Fig. 5), which could still be tolerated by NN data. However, even such a small change of the strength would increase the deuteron binding to $E_d^{\lambda=1.02} = -2.592$ MeV, in contradiction with the very precise experimental value. Also, ^{3}H would be more strongly bound, with $E_{^3H}^{\lambda=1.02} = -8.598$ MeV.

Summarizing, despite the fact that the SST cross sections are strongly dominated by the S-wave NN force components, modifications of their strengths cannot explain differences between theory and low-energy data for that configuration. Namely, those NN force components are very much restricted by available $2N$ and $3N$ data and their variations have to be considered with great caution.

III. RESULTS WITH CHIRAL *NN* POTENTIALS

From the available chiral NN interactions we choose four of the most advanced potentials which provide a satisfactory description of NN data in a large energy range. One is an older set of Bochum forces [31,32] developed up to fourth order (N^{3}LO) of chiral expansion. It reproduces experimental NN phase shifts in a wide energy range with an accuracy almost comparable to the high-precision (semi)phenomenological NN potentials. We employ five versions of that N^{3}LO chiral NN potential corresponding to different sets of cutoff parameters used to regularize the Lippmann-Schwinger equation and in spectral function regularization, namely (450,500) MeV, (450,700) MeV, (550,600) MeV, (600,500) MeV, and (600,700) MeV, denoted in the following by 201, 202, 203, 204, and 205, respectively.

Two other choices are the new-generation chiral NN potentials introduced and developed up to N^{4}LO by the Bochum-Bonn [39,40] and Idaho-Salamanca [41] groups. While in the Idaho-Salamanca force, the nonlocal momentum-space regularization was applied with a cutoff parameter Λ, in the Bochum-Bonn potential the one-pion and two-pion exchange contributions are regularized in coordinate space using the cutoff parameter R, and for the contact interactions a simple Gaussian nonlocal momentum-space regulator with the cutoff $\Lambda = 2R^{-1}$ was used. The Idaho-Salamanca N^{4}LO force is available for three values of the cutoff parameter $\Lambda = 450$, 500, and 550 MeV, while the semilocal coordinate-space regularized (SCS) chiral Bochum-Bonn potential has been developed for five cutoff parameters $R = 0.8$, 0.9, 1.0, 1.1, and 1.2 fm. Both versions provide a very good description of the NN data set (Idaho-Salamanca) or the phase shifts and mixing angles of the Nijmegen partial-wave analysis [42] (Bochum-Bonn), used to fix the low-energy constants (LECs) accompanying the NN contact interactions.

The last chiral potential considered here is the so-called semilocal momentum-space regularized (SMS) chiral potential of the Bochum group [43], developed up to fifth order (N^{4}LO) of chiral expansion and augmented by an additional (so-called N^{4}LO$^+$) version, including some sixth-order terms (the N^{4}LO Idaho-Salamanca potential is also augmented by the same Q^6 contact terms). In this $2N$ chiral force, a new momentum-space regularization scheme for the long-range contributions is employed, and a nonlocal Gaussian regulator for the minimal set of independent contact interactions is introduced. These new features have also been applied to the corresponding $3N$ forces at the N^{2}LO level [44]. This new family of semilocal chiral $2N$ potentials provides an outstanding description of the NN data and is available up to N^{4}LO$^+$ for five values of the cutoff $\Lambda = 350$, 400, 450, 500, and 550 MeV.

In Fig. 6 we show predictions of these NN potentials at $E = 13$ and 65 MeV as bands comprising the available range of cutoffs or regulator parameters for each of the four models. At 13 MeV the bands are very narrow and practically overlap with each other. Similarly to the (semi)phenomenological NN potentials, the chiral interactions also provide predictions for the SST cross sections at low energies that are very stable with respect to the type of the underlying interaction and its

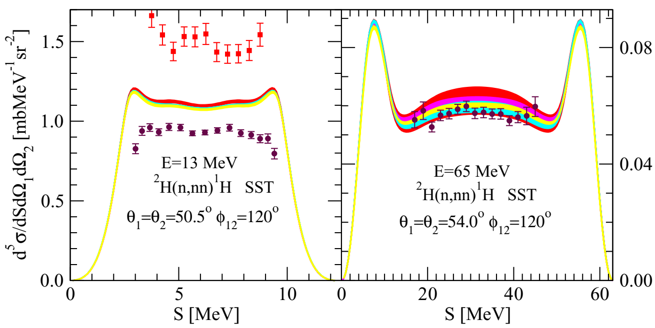

FIG. 6. The predicted SST cross sections by chiral NN potentials at incoming neutron laboratory energies $E = 13$ and 65 MeV. The red shaded band comprises five predictions of N^{3}LO chiral potentials (201, 202, 203, 204, 205) of Ref. [32] and the magenta band three predictions of N^{4}LO potentials of Ref. [41] with regulator parameters $\Lambda = 450, 500, 550$ MeV. The cyan band covers five predictions of the SCS N^{4}LO potential of Ref. [39] with regulator parameters $R = 0.8$, 0.9, 1.0, 1.1, 1.2 fm and the yellow band four predictions of the SMS N^{4}LO$^+$ potential of Ref. [43] with regulators $\Lambda = 400, 450, 500$, 550 MeV. For a description of the data points, see Fig. 2.

parameters as far as they provide a satisfactory description of the NN data. The predictions of the chiral potentials agree with those of (semi)phenomenological forces, leading to the same disagreement with the low-energy SST cross-section data.

As can be seen in Fig. 6, these bands are broadened at 65 MeV, especially for the older Bochum-Bonn potential [the red dark shaded band in Fig. 6], reflecting the increased dependence of the predictions on potential parameters at that energy as well as the worse description of NN data by the older Bochum-Bonn potential. The bands of SCS and SMS interactions are significantly constricted, in line with a good representation of the NN phase shifts by these potentials.

The applied chiral potentials differ not only in their regularization scheme. The older Bochum-Bonn potential leads to the deuteron wave function, which is quite different from those obtained with other chiral potentials [45]. Despite these differences the calculated low-energy SST cross sections are practically the same.

IV. RESULTS WITH CHIRAL 3N FORCES

First nonvanishing 3NF contributions appear at N^{2}LO [46,47] and contain, in addition to the 2π exchange term, two short-range contributions with the strength parameters c_D and c_E [48]. The latter two can be determined from the ^{3}H binding energy and the Nd differential cross-section minimum at about $E_{\rm lab} = 70$ MeV, which is the energy at which effects of 3NF start to appear in the Nd elastic-scattering cross section [4,36,44,49]. Specifically, first the so-called (c_D, c_E) correlation line is established, which for a particular chiral NN potential combined with a N^{2}LO 3NF yields values of (c_D, c_E), reproducing the ^{3}H binding energy. Then, a fit to the experimental data for the elastic Nd cross section is performed and the values of both strengths, c_D and c_E, are uniquely determined.

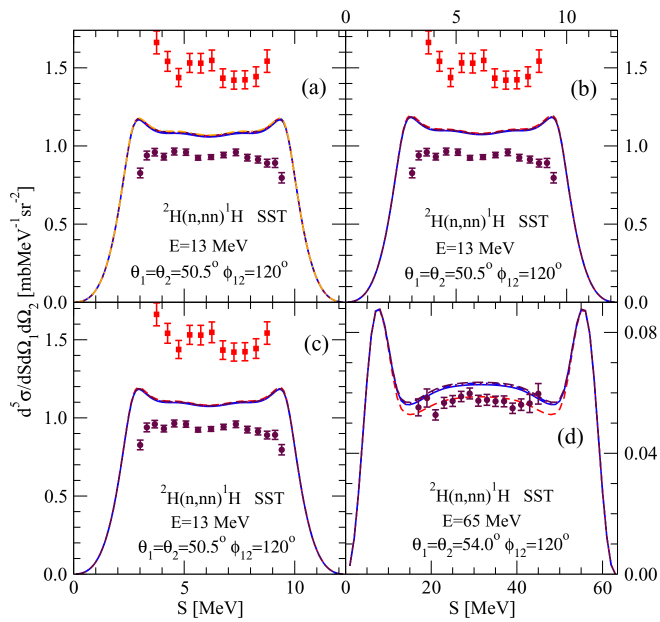

FIG. 7. Effects of N^{2}LO 3NF on SST cross section at $E = 13$ and 65 MeV when combined with chiral SCS NN potential at different orders of chiral expansion. The dashed red lines are predictions of the SCS NN potential with the regulator $R = 0.9$ fm at (a) N^{2}LO, (b) N^{3}LO, and (c), (d) N^{4}LO. Combining that potential with the N^{2}LO 3NF with four strengths of the contact terms from the correlation lines (c_D, c_E) leads to results shown by different curves: solid blue [(a) $(-4.0, 0.344)$, (b) $(4.0, 0.103)$, (c), (d) $(4.0, -0.270)$], dotted red [(a) $(-2.0, 0.131)$, (b) $(6.0, -0.960)$, (c), (d) $(6.0, -1.094)$], double-dotted-dashed blue [(a) $(0.0, -0.097)$, (b) $(8.0, -1.937)$, (c), (d) $(8.0, -2.032)$], and dashed maroon [(a) $(2.0, 0.345)$, (b) $(10.0, -3.063)$, (c), (d) $(10.0, -3.108)$]. For description of the data points see Fig. 2.

In Figs. 7(a)–7(c) we show predictions for the SST cross section at $E = 13$ MeV for the SCS chiral potential with the regularization parameter $R = 0.9$ fm at N^{2}LO, N^{3}LO, and N^{4}LO, respectively, combined with the N^{2}LO 3NF for four sets of the strength parameters taken from the corresponding correlation lines. Also, predictions of particular chiral potentials are shown by red dashed line. All lines practically overlap, showing that effects of N^{2}LO 3NF on 13 MeV SST cross section are negligible. The predicted cross section is insensitive to the order of the chiral NN potential used.

Effects of the N^{2}LO 3NF start to appear at 65 MeV [see Fig. 7(d)]. This is the energy region, where effects of 3NFs start to come into play also in elastic Nd scattering [4,36]. The overlapping predictions for four sets of strength combinations from the correlation line (c_D, c_E) shown in Fig. 7(d) indicates that the magnitude of 3NF effects in this energy range does not depend on strength values as far as they are taken from the correlation line.

To investigate further how effects of the N^{2}LO 3NF depend on the strengths of the contact terms we took the most precise chiral SMS potential at N^{4}LO$^+$ with the regulator $\Lambda = 450$ MeV and combined it with the N^{2}LO 3NF [48]. In Fig. 8 we show predictions for SST cross sections at $E = 13$ and 65 MeV for eight combinations of strengths taken from the

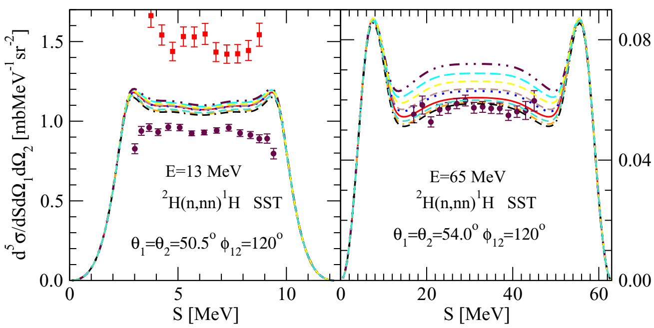

FIG. 8. SST cross sections at $E = 13$ and 65 MeV predicted by SMS chiral N^{4}LO$^+$ NN potential (the regulator parameter $\Lambda = 450$ MeV) alone (shown by dashed red lines) or combined with consistently regularized N^{2}LO 3NF with different strengths of the contact terms taken from the correlation line (c_D, c_E) and shown by lines: dotted blue (2.0,0.287), short dashed brown (4.0,0.499), long dashed cyan (15.0,1.362), dash-dotted orange (-15.0, -2.010), dash-double-dotted maroon (20.0,1.533), double-dash-dotted black (-20.0, 1.362), and short dashed turquoise (-10.0, -1.257). For a description of the data points, see Fig. 2.

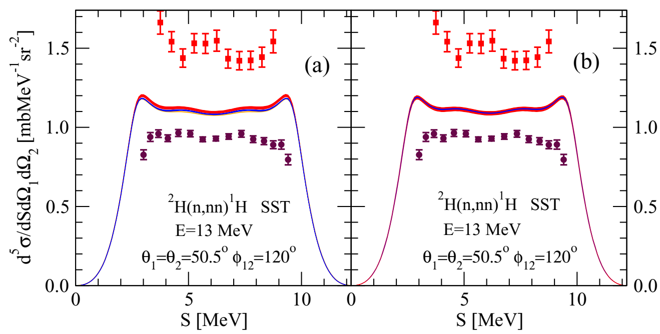

FIG. 9. (a) Effects of N^{3}LO 3NF, restricted to $3N$ total angular momenta $J = 1/2$ and $3/2$, with all long-range contributions with the exception of $1/m$ corrections and the omitted 2π-exchange contact term in the short-range part on the SST cross section at $E = 13$ MeV. The red band in panel (a) comprises predictions of five chiral N^{3}LO Bochum-Bonn potentials (201–205). Combining them with N^{3}LO 3NF with strengths of the contact terms determined by the correlation line (c_D, c_E) and requirement to reproduce $^2a_{nd}$ leads to the blue band. The orange solid line is the prediction of the CD Bonn potential. In panel (b), the same is shown for chiral Bochum-Bonn potentials and 3NF at N^{2}LO. In this case, the N^{2}LO 3NF acted up to $J = 7/2$. For a description of the data points, see Fig. 2.

correlation line (c_D, c_E). Again, in spite of a very wide range of c_D values, taken between $c_D = -20$ and $c_D = +20$, the predicted 13 MeV cross sections are found to lie within a relatively narrow band. Contrary to that, at 65 MeV a very broad range of predictions is seen, confirming the observation that, in this energy region, 3NF effects become important.

One may now raise the question of the role of 3NF components from higher chiral orders and their impact on the SST cross section. The necessary work to derive the chiral 3NFs at N^{3}LO has been done in Refs. [50,51] using dimensional regularization. At that order, five different topologies contribute to the 3NF. Three of them are of long-range character [50] and are given by two-pion (2π) exchange graphs, by two-pion-one-pion (2π-1π) exchange graphs, and by the so-called ring diagrams. They are supplemented by the short-range one-pion-exchange contact (1π contact) and two-pion-exchange contact (2π contact) terms [51]. The 3NF at N^{3}LO order does not involve any new unknown low-energy constants (LECs), see, however, a related discussion in Ref. [52], and depends only on two parameters, c_D and c_E, that parametrize the leading one-pion-contact term and the $3N$ contact term appearing already at N^{2}LO. Their values need to be fixed at a given order from a fit to few-nucleon data, as in the N^{2}LO case.

In the first preliminary investigation of N^{3}LO 3NF effects [45] we considered the action of the 3NF only in $3N$ states with the total $3N$ angular momenta $J = 1/2$ and $3/2$ and included all long-range contributions with the exception of $1/m$ corrections. Additionally, the 2π-exchange contact term was omitted in the short-range part of 3NF. The strengths parameters c_E and c_D were determined at that time from the correlation line, and the nd doublet scattering length $^2a_{nd}$ was used in addition to the ^{3}H binding energy to uniquely determine both values.

In Fig. 9(a) we show the SST cross sections at 13 MeV in form of a red band comprising five predictions of the N^{3}LO Bochum-Bonn potentials (versions 201–205). Combining these potentials with the N^{3}LO chiral 3NF gives the blue band. For the sake of comparison, the CD Bonn prediction is also shown by the orange solid line. In Fig. 9(b), the corresponding predictions at N^{2}LO are also presented. It again turns out that the cross section for the SST configuration of the nd breakup is very stable with respect to the underlying dynamics. Not only (semi)phenomenological potentials, alone or combined with standard $3N$ forces, provide practically the same SST cross sections. Also the chiral $2N$ forces supplemented by the N^{3}LO 3NF without relativistic $1/m$ corrections and short-range 2π-contact term yield similar predictions and cannot explain the discrepancy between the theory and the data found for the low-energy SST configurations. Notice further that a consistent regularization of the 3NF beyond N^{2}LO has not yet been achieved, see Ref. [53].

Due to the restriction to the low total $3N$ angular momenta this result has to be confirmed. A systematic investigation of effects of the 3NF beyond N^{2}LO is the main aim of the LENPIC collaboration [49].

At fifth order (N^{4}LO), the chiral 3NF comprises thirteen purely short-range operators [54] in addition to the long- and intermediate-range interactions generated by pion-exchange diagrams [55,56]. In an exploratory study of Ref. [57], effects of these subleading short-range terms were investigated in pd scattering below $E_{\rm lab} = 3$ MeV within a hybrid approach based on phenomenological two- and three-nucleon forces.

To get insight into the expected 3NF effects on SST cross sections from these N^{4}LO short-range 3NF contributions we choose two out of the thirteen terms, namely, the isoscalar central and spin-orbit interactions coming with strengths c_{E_1} and c_{E_7}, respectively [48,54] and add them to the N^{2}LO 3NF. In Fig. 10, we show predictions for the SST cross section at $E = 13$ and 65 MeV for the chiral SMS N^{4}LO$^+$ potential with regularization parameter $\Lambda = 450$ MeV combined with

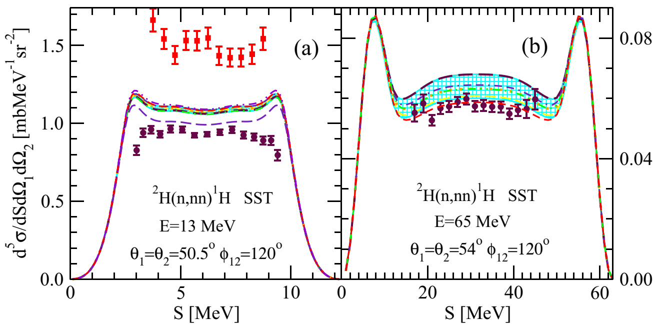

FIG. 10. SST cross sections at $E = 13$ and 65 MeV predicted by the chiral SMS N^{4}LO$^+$ NN potential with the regulator parameter $\Lambda = 450$ MeV alone (the long dashed yellow lines) or combined with 3NF comprising N^{2}LO and two out of thirteen N^{4}LO contact terms, with strengths of the contact terms from the correlation line ($c_D, c_E, c_{E_1}, c_{E7}$). The results with 3NF are shown by the following lines: dotted orange (2.741,0.367,0.0,0.0), dash-double-dotted turquoise (10.818, −0.295, −4.0, 0.0), long dashed maroon (−11.977, −0.969, 4.0, 0.0), double-dash-dotted indigo (10.471, 1.079, 0.0, −4.0), and dash-double-dotted green (−8.205, −1.002, 0.0, 2.0). The cyan shaded band covers region of predictions given by five above and three additional sets of strengths: (6.971, 0.207, −2.0, 0.0), (8.533, 0.925, 0.0, −2.0), (3.133,0.041,2.0,0.0). For comparison, the short dashed red line is also drawn which is the prediction of the SCS N^{4}LO potential with the regulator parameter $R = 0.9$ fm. In panel (a), two additional lines are drawn which correspond to the combinations of strengths (c_D, c_E) outside the correlation line, namely indigo long dashed: (2.0,1.433) and red dash-double-dotted: (2.0, −1.433). For a description of the data points, see Fig. 2.

that 3NF for a set of eight combinations of strengths from the correlation lines ($c_D, c_E, c_{E_1}, c_{E_7}$) for fixed values of c_{E_1} and c_{E_7}. For five of these combinations the lines of predictions are also drawn. It is seen that the inclusion of the c_{E_1} and c_{E_7} terms has a negligible effect on the 13 MeV SST cross section, and the predicted cross sections essentially coincide with each other and with the results of SCS N^{4}LO and SMS N^{4}LO$^+$ potentials alone. Again, at 65 MeV, a wide spread of predictions indicates significant effects of the 3NF at this energy.

The observed discrepancy between theoretical predictions and the *nd* and *pd* low-energy SST cross-section data thus indeed appears to be puzzling. Due to the observed strong stability of the low-energy space-star cross sections to the underlying dynamics it seems very unlikely that this puzzle can be resolved by the inclusion of omitted N^{3}LO terms or remaining N^{4}LO and higher-order contributions to the 3NF. We checked for a combination of SMS N^{4}LO$^+$ NN and N^{2}LO 3NF that even removing the requirement to reproduce the ^{3}H binding energy does not help to come into the vicinity of the 13 MeV *nd* SST cross-section data. Namely, taking strengths $c_D = 2.0$ and $c_E = 0.287$ from the correlation line and increasing c_E to $c_E = 1.433$ lowers the predicted cross sections and brings them close to *pd* SST data (see long dashed indigo line in Fig. 10). For the combination of strengths $c_D = 2.0$, $c_E = 1.433$, ^{3}H is strongly bound with $E_{^3H} = -10.783$ MeV. However, decreasing the c_E value and even changing its sign does not have any significant effect on the predicted cross section, which remains close to the stable region of predictions for strength values from the correlation line (see Fig. 10 and the red dash-double-dotted line, which is a prediction for $c_D = 2.0$ and $c_E = -1.433$). For the combination of strengths $c_D = 2.0$, $c_E = -1.433$, ^{3}H is bound with $E_{^3H} = -6.792$ MeV.

V. DISCUSSION OF THE LOW-ENERGY DISCREPANCY

The results presented support the conjecture that 3NF effects are not responsible for the discrepancies between data and theory in the low-energy SST cross sections. One could argue that, perhaps, modifications of the $^1S_0$ and/or $^3S_1 - {}^3D_1$ NN force components, more refined than a simple change of their strengths, would provide an explanation for at least *pd* SST low-energy cross-section data. However, this seems to be difficult since there is no room for modifications of *np* and *pp* forces compatible with NN data [42,58,59]. In spite of the fact that the *pd* SST discrepancy is relatively small (≈10 %) in comparison with the *nd* SST discrepancy, since the theoretical predictions lie well outside statistical error bars and the systematic errors are claimed to be small [19], it presents a significant discrepancy. A dedicated *pd* SST measurement aiming to determine precise normalization of the SST cross sections would help to put some light on this discrepancy. Even larger is the discrepancy to *nd* SST data and between *pd* and *nd* data themselves. However, due to the strong insensitivity of low-energy SST cross sections to the underlying dynamics it seems rather unlikely that any conceivable charge symmetry breaking mechanism in the NN and/or 3N force would be able to explain the difference between *pd* and *nd* SST data and allow us to describe *nd* data. This situation poses an interesting puzzle for theory and its solution has to be probably sought in some exotic mechanism contributing to the *nd* breakup and irrelevant for the *pd* one. When looking for such a mechanism one could consider the contributions of hypothetical bound state of two neutrons in the state $^1S_0$ to a region of SST breakup phase-space. Such contributions could create in *nd* SST measurements additional background originating from accidental coincidences between breakup neutrons and dineutrons produced in *nd* scattering, increasing thus the measured cross section. That such a scenario is conceivable follows from the fact that detection of neutrons in *nd* SST measurements was performed using liquid scintillators with pulse-shape discrimination and their energy was determined by the time-of-flight technique [12]. Such a detection system does not distinguish between dineutrons and breakup neutrons. As a result, accidental coincidences between breakup neutrons and dineutrons could appear in the region of SST phase space which cannot be distinguished from true events by the applied measurement technique. The kinetic energy assigned to dineutron when using such an experimental arrangement, which is determined by time-of-flight measurement of its velocity, will be in consequence twice as small as its real kinetic energy. To be specific, assuming that dineutron is bound by $E_b^{\rm din} = -0.144$ MeV (which corresponds to the factor $\lambda_{^1S_0} = 1.21$) would lead at incoming neutron laboratory energy $E = 13$ MeV to the energy of

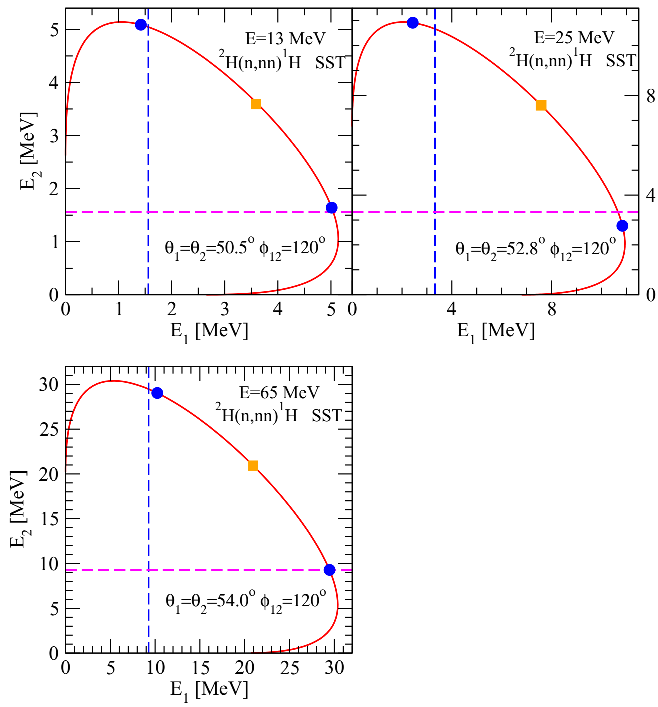

FIG. 11. Position of ^{2}H$(n, nn)\,^1$H breakup events (S curve) in the laboratory kinetic-energy plane E_1-E_2 of two detected in coincidence neutrons for SST configurations at $E = 13$, 25, and 65 MeV. The dashed lines show half of the energy of the outgoing dineutron from ^{2}H$(n,\text{dineutron})\,^1$H reaction at the laboratory angle of the corresponding SST geometry. The position on the S curve where the SST condition is fulfilled is shown by squares and the range of the S curve covered by *nd* (*pd*) SST data is indicated by dots.

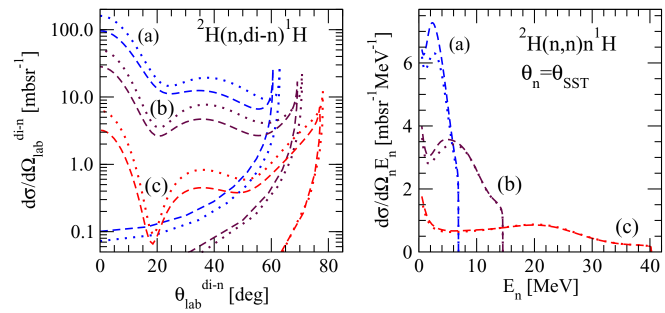

FIG. 12. The angular distributions of dineutrons and the energy spectra of outgoing neutrons from incomplete breakup reaction ^{2}H$(n, n)n\,^1$H for a laboratory angle of the detected neutron equal to the SST configuration angle, predicted by the CD Bonn potential with a $^1S_0$ *nn* force component modified by increasing its strength by a factor λ to get two neutrons bound. The blue dashed line corresponds to $\lambda = 1.21$ with dineutron binding energy $E_b^{\text{din}} = -0.144$ MeV and the dashed-dotted line to $\lambda = 1.3$ with $E_b^{\text{din}} = -0.441$ MeV. Panels (a)–(c) are predictions for incoming neutron laboratory energies $E = 13$, 25, and 65 MeV, respectively.

outgoing dineutrons from ^{2}H$(n,\text{dineutron})\,^1$H reaction at the laboratory angle of the SST configuration, $\theta = 50.5^\circ$, $E_{\text{lab}}^{\text{din}} =$ 3.12 MeV and its energy detected by the TOF system will be 1.56 MeV. In Fig. 11, positions of breakup events (S curve) in the plane of kinetic energies E_1-E_2 of two outgoing neutrons detected in coincidence are shown together with the positions of dineutron energies determined by the detection system for SST configurations at $E = 13$, 19, and 65 MeV. Also, the range of S curve covered by data is indicated by two circles. Since at 13 MeV dineutrons would come nearest to the SST region, the data at that energy would be influenced most by the assumptive background of accidental coincidences. The intensity of accidental coincidences depends on the number of neutrons or dineutrons arriving at detectors, which is determined by the energy spectra of outgoing neutrons in incomplete $d(n, n)np$ breakup and by laboratory angular distribution of dineutrons from the ^{2}H$(n,\text{dineutron})\,^1$H reaction. The predictions for these quantities based on solutions of the 3N Faddeev equation with a modified (in the $^1S_0$ partial wave) CD Bonn potential [37] at the above considered three energies are shown in Fig. 12. Since the cross section for dineutron production is comparable to the cross section for production of neutrons in incomplete *nd* breakup, it indeed seems plausible that accidental coincidences could impact the measured low-energy SST cross sections. Rapid diminishing of the dineutron production with energy (see Fig. 12) would also explain the implied decrease of the discrepancy between *nd* SST data and theory seen in Fig. 1 for higher energies.

One could argue that, even with the applied neutron detection system, it should be possible to distinguish between hypothetical dineutrons from ^{2}H$(n,\text{dineutron})\,^1$H reaction and the breakup neutrons. Namely, since the dineutron detected in a neutron detector is produced in a two-body process, it must be accompanied by a proton of specific energy, flying at a definite angle. Therefore a coincidence between the neutron detector and a proton detector placed at that angle would provide the required information necessary to separate the dineutron and neutron events. However, even if this information was available, such a separation would be hindered or even precluded, as demonstrated in Fig. 13. In the left column for $E = 13$ and 65 MeV we show by dots the locations of dineutron-proton coincidences in the plane of kinetic energies of dineutron (E_1) and proton (E_2), when the neutron detector is placed at the laboratory angle of the SST configuration and the proton detector at the angle of the outgoing proton from the ^{2}H$(n,\text{dineutron})\,^1$H reaction. Also the S curves are displayed, along which the neutron-proton coincidences from the ^{2}H$(n, np)n$ reaction are located. In the right column of Fig. 13, the cross sections for these particular ^{2}H$(n, np)n$ complete breakup configurations are shown together with the positions (marked with dashed lines) of the points on the S curves closest to the location of the dineutron-proton coincidences. At those points two outgoing breakup neutrons have equal momenta and strongly interact, which leads to characteristic final-state-interaction peaks in the cross section. It is clear that, due to finite angular and energy resolutions of the experimental setup causing the actual overlap of these two kinds of events, even with such an "extended" detection system one would not be able to isolate the dineutron events. Therefore, new measurements of the low-energy *nd* SST cross sections as well as a measurement of *nd* SST at $E = 65$ MeV, using a detection system able to distinguish between neutrons and

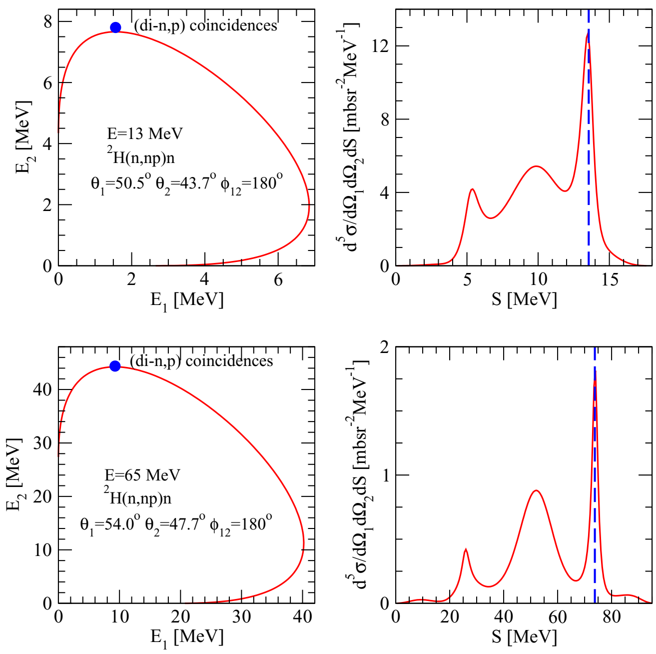

FIG. 13. (left column) The locus (S curve) of the final laboratory kinetic energy of neutrons (E_1) and protons (E_2) for the ^{2}H(n, np)n breakup reaction at the incoming neutron energies $E = 13$ and 65 MeV. The neutron angle corresponds to the SST geometry and the proton angle is equal to the angle of the outgoing proton in the ^{2}H(n, dineutron) ^{1}H two-body reaction, with dineutrons emerging at the same angle as the neutrons from the breakup reaction. The dots show unique positions of the dineutron-proton coincidences. (right column) The cross sections for these complete breakup configurations calculated with the chiral SMS N^{4}LO$^+$ *NN* potential with the regulator parameter $\Lambda = 450$ MeV (solid line). The arc-length value S of the point closest to the location of the dineutron-proton coincidences is marked with the dashed line. At that point, two outgoing breakup neutrons have equal momenta and strongly interact.

hypothetical dineutrons, like the one proposed in Ref. [60], would be very welcome.

We would like to emphasize that, even with the standard detection system, a measurement of the *nd* SST at 65 MeV would be very desired. Smaller contributions of hypothetical dineutron events to the background at this energy and, as shown in Fig. 4, a significant increase of the 65 MeV *nd* SST cross section by dineutrons absent in the *pd* reaction, would made such data very important for testing the dineutron hypothesis.

VI. SUMMARY AND CONCLUSIONS

In this investigation we performed a comprehensive analysis of the available SST *Nd* breakup cross-section data using high-precision (semi)phenomenological *NN* potentials alone or combined with the standard 3*N* forces as well as selected chiral forces. Four different chiral *NN* potentials including the most precise SMS N^{4}LO$^+$ of Ref. [43] have been applied alone or in combination with chiral 3NF's at different orders of chiral expansion. The main results are summarized as follows:

(i) The available *nd* SST data cover the range of incoming neutron lab. energies between $E = 10$–25 MeV while the *pd* data were measured for proton energies in a region $E = 10$–65 MeV. The experiments were performed by different groups using different experimental arrangements or techniques. When at a particular energy, several *pd* or *nd* data sets are available, the data from different measurements are consistent with each other.

(ii) Using (semi)phenomenological *NN* potentials alone or accompanied by the TM99 or Urbana IX 3NF one is not able to explain the low-energy SST *pd* and *nd* SST data. All theoretical predictions practically overlap in *nd* and *pd* systems with *pd* data overestimated by ≈10% and *nd* data underestimated by ≈20%–30%. The discrepancies between theory and data diminish with increasing energy of the incoming nucleon. At $E = 65$ MeV, *NN* force predictions agree with the *pd* SST cross sections, while inclusion of 3NF provides a slight overestimation of the data.

(iii) Predicted low-energy SST cross sections based on different chiral *NN* potentials are independent of the type of regularization used or from the regularization parameters and are practically identical to predictions of (semi)phenomenological interactions. At $E = 65$ MeV that independence starts to be lost.

(iv) Adding the considered chiral 3NF at different orders of chiral expansion has no significant influence on the SST cross sections at low energy. Even a broader range of strengths from the correlation line (c_D, c_E) for N^{2}LO 3NF contact terms yields practically the same low-energy SST cross sections. Again, at $E =$ 65 MeV, this stability with respect to changes of strengths vanishes and 3NF effects come into play.

(v) The low-energy SST cross sections originate practically from $^1S_0$ and $^3S_1 - {}^3D_1$ *NN* force components. Changes introduced by a simple multiplication of the corresponding matrix elements by a factor λ could explain the SST *pd* data but not *nd* data. However, the required changes of the $^1S_0$ and/or $^3S_1 - {}^3D_1$ are excluded by the *NN* data and/or by the ^3H binding energy.

(vi) In view of the astonishing stability of the low-energy SST cross sections to the underlying dynamics it seems very unlikely that a charge symmetry breaking mechanism of any conceivable kind in 2*N* or 3*N* forces could be able to explain the low-energy *nd* SST cross sections. The explanation of the *nd* data should be thus sought in some exotic phenomena, such as, e.g., the hypothetical bound state of two neutrons. Supposable existence of the dineutron would provide additional background in the region of the SST breakup phase space, which could not be discerned in measurements performed so far.

Further investigations and theoretical as well as experimental efforts are required to solve that low-energy SST puzzle. From the experimental side, measurements of *nd* SST cross sections at low-energies with experimental arrangement able to discern supposable dineutron background would be needed. Also, dedicated *pd* SST measurement directed to determine precise normalization of SST cross sections would be welcome. From the theoretical side, efforts to fully include in $3N$ continuum calculations consistently regularized N^{3}LO and N^{4}LO 3NF components are required. This is the aim of the LENPIC project.

ACKNOWLEDGMENTS

This study has been performed within Low Energy Nuclear Physics International Collaboration (LENPIC) project and was supported by the Polish National Science Center under Grant No. 2016/22/M/ST2/00173, by Deutsche Forschungsgemeinschaft (DFG) and the Natural Science Foundation of China (NSFC) through funds provided to the Sino-German CRC 110 “Symmetries and the Emergence of Structures in QCD” (NSFC Grant No. 11621131001, DFG Project-Id 196253076-TRR 110) and by Bundesministerium für Bildung und Forschung (BMBF), Grant No. 05P18PCFP1. The numerical calculations were performed on the supercomputer cluster of the JSC, Jülich, Germany. We would like to thank other members of the LENPIC Collaboration for interesting discussions and A. Nogga and K. Hebeler for providing us with matrix elements of N^{2}LO chiral 3NFs.

[1] W. Glöckle, H. Witała, D. Hüber, H. Kamada, and J. Golak, Phys. Rep. **274**, 107 (1996).
[2] A. Deltuva, K. Chmielewski, and P. U. Sauer, Phys. Rev. C **67**, 034001 (2003).
[3] A. Kievsky, M. Viviani, and S. Rosati, Phys. Rev. C **52**, R15 (1995).
[4] H. Witała, W. Glöckle, J. Golak, A. Nogga, H. Kamada, R. Skibiński and J. Kuroś-Żołnierczuk, Phys. Rev. C **63**, 024007 (2001), and references therein.
[5] J. Kuroś-Żołnierczuk, H. Witała, J. Golak, H. Kamada, A. Nogga, R. Skibiński, and W. Glöckle, Phys. Rev. C **66**, 024003 (2002).
[6] M. Stephan, K. Bodek, J. Krug, W. Lübcke, S. Obermanns, H. Rühl, M. Steinke, D. Kamke, H. Witała, Th. Cornelius and W. Glöckle, Phys. Rev. C **39**, 2133 (1989).
[7] K. Gebhardt *et al.*, Nucl. Phys. A **561**, 232 (1993).
[8] R. Macri, Ph.D. thesis, Duke University, 2004 (unpublished).
[9] J. Strate, K. Geissdörfer, R. Lin, J. Cub, E. Finckh, K. Gebhardt, S. Schindler, H. Witała, W. Glöckle, and T. Cornelius, J. Phys. G: Nucl. Phys. **14**, L229 (1988).
[10] J. Strate *et al.*, Nucl. Phys. A **501**, 51 (1989).
[11] H. R. Setze, C. R. Howell, W. Tornow, R. T. Braun, W. Glöckle, A. H. Hussein, J. M. Lambert, G. Mertens, C. D. Roper, F. Salinas, I. Slaus, D. E. Gonzalez Trotter, B. Vlahovic, R. L. Walter, and H. Witała, Phys. Lett. B **388**, 229 (1996).
[12] H. R. Setze *et al.*, Phys. Rev. C **71**, 034006 (2005).
[13] A. Crowell, Ph.D. thesis, Duke University, 2001 (unpublished).
[14] A. H. Couture, T. B. Clegg, S. Tajima, C. R. Howell, B. Fallin, J. H. Esterline, A. S. Crowell, B. J. Crowe, D. M. Markoff, L. C. Cumberbatch, R. S. Pedroni, and H. Witała, Phys. Rev. C **85**, 054004 (2012).
[15] Z. Zhou *et al.*, Nucl. Phys. A **684**, 545 (2001).
[16] R. Grossmann, G. Nitzsche, H. Patberg, L. Sydow, S. Vohl, H. Paetz gen. Schieck, J. Golak, H. Witała, W. Glöckle, and D. Hüber, Nucl. Phys. A **603**, 161 (1996).
[17] G. Rauprich, S. Lemaître, P. Nießen, K. R. Nyga, R. Reckenfelderbäumer, L. Sydow, H. Paetz gen. Schieck, H. Witała, and W. Glöckle, Nucl. Phys. A **535**, 313 (1991).
[18] T. Ishida *et al.*, Mod. Phys. Lett. A **18**, 436 (2003).
[19] K. Sagara, Few-Body Syst. **48**, 59 (2010).
[20] H. Patberg, R. Grossmann, G. Nitzsche, L. Sydow, S. Vohl, H. P. Schieck, J. Golak, H. Witała, W. Glöckle, and D. Hüber, Phys. Rev. C **53**, 1497 (1996).
[21] J. Zejma *et al.*, Phys. Rev. C **55**, 42 (1997).
[22] M. Lacombe, B. Loiseau, J. M. Richard, R. Vinh Mau, J. Cote, P. Pires, and R. de Tourreil, Phys. Rev. C **21**, 861 (1980); Phys. Rev. D **12**, 1495 (1975).
[23] R. Machleidt, R. Holinde, and Ch. Elster, Phys. Rep. **149**, 1 (1987).
[24] R. B. Wiringa, V. G. J. Stoks, and R. Schiavilla, Phys. Rev. C **51**, 38 (1995).
[25] R. Machleidt, Phys. Rev. C **63**, 024001 (2001).
[26] V. G. J. Stoks, R. A. M. Klomp, C. P. F. Terheggen, and J. J. de Swart, Phys. Rev. C **49**, 2950 (1994).
[27] D. Hüber H. Kamada, H. Witała, and W. Glöckle, Acta Phys. Pol. B **28**, 1677 (1997).
[28] B. S. Pudliner V. R. Pandharipande, J. Carlson, S. C. Pieper, and R. B. Wiringa, Phys. Rev. C **56**, 1720 (1997).
[29] S. A. Coon and H. K. Han, Few-Body Syst. **30**, 131 (2001).
[30] A. Deltuva, A. C. Fonseca, and P. U. Sauer, Phys. Rev. C **72**, 054004 (2005).
[31] E. Epelbaum, W. Glöckle, and U.-G. Meißner, Nucl. Phys. A **747**, 362 (2005).
[32] E. Epelbaum, Prog. Part. Nucl. Phys. **57**, 654 (2006).
[33] R. Machleidt and D. R. Entem, Phys. Rep. **503**, 1 (2011).
[34] H. Witała, T. Cornelius, and W. Glöckle, Few-Body Syst. **3**, 123 (1988).
[35] W. Glöckle, *The Quantum Mechanical Few-Body Problem* (Springer Verlag, Berlin, Heidelberg, New York, Tokyo, 1983).
[36] H. Witała, W. Glöckle, D. Hüber, J. Golak, and H. Kamada, Phys. Rev. Lett. **81**, 1183 (1998).
[37] H. Witała and W. Glöckle, Phys. Rev. C **85**, 064003 (2012).
[38] C. van der Leun and C. Alderlisten, Nucl. Phys. A **380**, 261 (1982).
[39] E. Epelbaum, H. Krebs, and U.-G. Meißner, Eur. Phys. J. A **51**, 53 (2015).
[40] E. Epelbaum, H. Krebs, and U.-G. Meißner, Phys. Rev. Lett. **115**, 122301 (2015).
[41] D. R. Entem, R. Machleidt, and Y. Nosyk, Phys. Rev. C **96**, 024004 (2017).
[42] V. G. J. Stoks, R. A. M. Klomp, M. C. M. Rentmeester, and J. J. de Swart, Phys. Rev. C **48**, 792 (1993).
[43] P. Reinert, H. Krebs, and E. Epelbaum, Eur. Phys. J. A **54**, 86 (2018).
[44] P. Maris *et al.* (LENPIC Collaboration), Phys. Rev. C **103**, 054001 (2021).

[45] H. Witała, J. Golak, R. Skibiński, and K. Topolnicki, J. Phys. G **41**, 094011 (2014).

[46] U. van Kolck, Phys. Rev. C **49**, 2932 (1994).

[47] E. Epelbaum, A. Nogga, W. Glöckle, H. Kamada, Ulf-G. Meißner, and H. Witała, Phys. Rev. C **66**, 064001 (2002).

[48] E. Epelbaum *et al.*, Eur. Phys. J. A **56**, 92 (2020).

[49] E. Epelbaum *et al.* (LENPIC Collaboration), Phys. Rev. C **99**, 024313 (2019).

[50] V. Bernard, E. Epelbaum, H. Krebs, and Ulf-G. Meißner, Phys. Rev. C **77**, 064004 (2008).

[51] V. Bernard, E. Epelbaum, H. Krebs, and Ulf-G. Meißner, Phys. Rev. C **84**, 054001 (2011).

[52] L. Girlanda, A. Kievsky, L. E. Marcucci, and M. Viviani, Phys. Rev. C **102**, 064003 (2020).

[53] E. Epelbaum, H. Krebs, and P. Reinert, arXiv:1911.11875 [nucl.th].

[54] L. Girlanda, A. Kievsky, and M. Viviani, Phys. Rev. C **84**, 014001 (2011); **102**, 019903(E) (2020).

[55] H. Krebs, A. Gasparyan, and E. Epelbaum, Phys. Rev. C **85**, 054006 (2012).

[56] H. Krebs, A. Gasparyan, and E. Epelbaum, Phys. Rev. C **87**, 054007 (2013).

[57] L. Girlanda, A. Kievsky, M. Viviani, and L. E. Marcucci, Phys. Rev. C **99**, 054003 (2019).

[58] R. N. Pérez, J. E. Amaro, and E. R. Arriola, Phys. Rev. C **88**, 064002 (2013); **91**, 029901(E) (2015).

[59] P. Reinert, H. Krebs, and E. Epelbaum, Phys. Rev. Lett. **126**, 092501 (2021).

[60] K. Bodek, Few-Body Syst. **55**, 713 (2014).